# Open Research Online

## Multiscale Measurements of Residual Stress in a Low-Alloy Carbon Steel Weld Clad with IN625 Superalloy

## Journal Item

For guidance on citations see FAQs.

## oro.open.ac.uk

## Materials Performance and Characterization

G. Benghalia,[1] S. Rahimi,[2] J. Wood,[3] H. Coules,[4] and S. Paddea[5]

# Multiscale Measurements of Residual Stress in a Low-Alloy Carbon Steel Weld Clad with IN625 Superalloy

G. Benghalia,[1] S. Rahimi,[2] J. Wood,[3] H. Coules,[4] and S. Paddea[5]

# Multiscale Measurements of Residual Stress in a Low-Alloy Carbon Steel Weld Clad with IN625 Superalloy

[1] Advanced Forming Research Centre, University of Strathclyde, 85 Inchinnan Dr., Renfrew PA4 9LJ, United Kingdom (Corresponding author), e-mail: gladys.benghalia@strath.ac.uk, https://orcid.org/0000-0003-3754-5269

[2] Advanced Forming Research Centre, University of Strathclyde, 85 Inchinnan Dr., Renfrew PA4 9LJ, United Kingdom

[3] Department of Mechanical & Aerospace Engineering, University of Strathclyde, James Weir Building, 75 Montrose St., Glasgow G1 1XJ, United Kingdom

[4] Department of Mechanical Engineering, University of Bristol, Queen's Building, University Walk, Bristol BS8 1TR, United Kingdom

[5] Stressmap, The Open University, Venables Building, Walton Hall, Milton Keynes MK7 6AA, United Kingdom

### ABSTRACT

Fatigue fracture is one of the major degradation mechanisms in the low-alloy 4330 carbon steel pumps that are utilized in the hydraulic fracturing process operating under cyclic loading conditions. A weld cladding technology has been developed to improve the ability of these components to resist fatigue crack initiation by cladding them with a secondary material. This process introduces a residual stress profile into the component that can be potentially detrimental for fatigue performance. The cladding technology under examination is a low-alloy 4330 carbon steel substrate weld that is clad with the nickel-chromium–based superalloy IN625 and is investigated herein using several experimental residual stress measurement techniques. Understanding the magnitude and distribution of residual stress in weld clad components is of the utmost importance to accurately assess the performance of the component in service. This study summarizes the results of residual stress measurements that were determined using X-ray diffraction, i.e., hole drilling based on electronic speckle pattern interferometry, deep-hole drilling, and the contour method, to obtain the residual stress distributions from the surface of the weld clad, through the clad layer, and into the substrate material. The results of deep-hole drilling and the contour method show large-scale tensile residual stress in the clad layer and compressive residual stress in the majority of the substrate. However, the X-ray diffraction and hole drilling methods indicate the presence of short-scale compressive residual stress on the surface and near the surface of the clad layer. It was shown that these

measurement techniques are complementary in assessing the residual stress profile throughout the entire component.

## Keywords

weld cladding, residual stress, X-ray diffraction, hole drilling, electronic speckle pattern interferometry, deep-hole drilling, contour method, 4330 carbon steel, IN625 superalloy

## Introduction

Low-alloy carbon steel, such as the 4330 investigated herein, is commonly utilized for its high strength and ability to enhance an array of properties, depending on the microstructure, which can be controlled by the cooling rate of the often hot-forged part. Slow furnace cooling or the use of insulation, as opposed to air cooling, decreases the likelihood of stress-induced cracking, whereas intercritical and double-hardening heat treatment can result in improved toughness [1,2]. Regardless of the measures taken to ensure appropriate material properties, the application of the component in operation poses several critical issues. For instance, during the hydraulic fracturing process, the pump bodies, which are typically made from carbon steel, are subjected to cyclic loading conditions alongside exposure to corrosive media and are therefore prone to various environmentally assisted degradation mechanisms, such as corrosion and erosion. These mechanisms can greatly reduce fatigue life, as, for example, 4140 heat-treated steel is shown to experience accelerated fatigue fracture by a factor of 3–4 in a corrosive environment [3]. Although components may be subjected to cyclic loading at stress levels below the yield strength, crack initiation and propagation can occur at applied stresses much lower than the yield point due to stress concentration that is caused by stress raisers and features in the component's design or residual stresses that remain in the part from the manufacturing process. The evaluation of material fatigue performance is crucial for structural integrity because 90 % of service failures in metals can be attributed to fatigue-based failures [4].

Weld overlay cladding can be achieved using hot-wire Gas Tungsten Arc Welding (GTAW) by depositing a layer of the clad material onto a substrate and creating a bond between the two materials. Manufacturing the entire component using a material with improved corrosion resistance is unlikely to provide an advantageous solution that is economically feasible. Applying a weld clad material with superior properties on a less resistant substrate is an alternative, economically viable approach to improving mechanical performance and corrosion and erosion resistance, providing an all-encompassing solution for the performance of components operating in such environments. Welding of structures is a common practice, wherein the welding process typically results in the generation of tensile residual stress that can have negative effects on the performance and structural integrity of the structure by providing sufficient driving force for crack initiation and propagation [5]. The presence of compressive residual stress can improve stress-corrosion cracking resistance and corrosion performance [6], as well as increase fatigue strength [7]. Shortening the crack initiation stage is a danger of the welding process, along with modification of the material properties of the substrate.

Residual stresses, present in parts in the absence of external applied loads or constraints, arise from misfits between different regions, such as heterogeneous plastic deformations, different crystallographic structures and thermal expansion coefficients [8]. The magnitude and distribution of these self-equilibrating elastic stresses require knowledge of

the key process variables, such as heat treatment [9], mechanical work [10], heterogeneous plastic deformation [11,12], or welding [13], that the component experiences during its manufacture. Thermal expansion constraints and nonuniform heating and cooling all induce residual stresses of different scales; thus, processes like forging, quenching, welding, and brazing cause dissimilarity in the material [14]. Likewise, chemical reactions, volume changes, and phase transformations either generate residual stress or influence the existing residual stress field [15–17]. Residual stresses can be categorized as macro- and micro-residual stresses; macrostresses being those with wavelengths comparable to the size of the component, while microstresses are in the region of grain and atomic scales [7]. Both macro- and microstresses may be present in a component; additionally, the former is classified as Type I, and the latter can be divided into Types II (i.e., at grain level) and III (i.e., at atomic level) residual stresses.

In weld cladding, residual stress will arise because of mechanical, thermal, and chemical mechanisms with the accompanying microstructures and, in turn, the nature of the residual stress is dependent on the degree of material dissimilarity [18]. It is common for welding and similar thermal processes to induce a complex residual stress field with potentially sharp stress gradients [19–21]. Thermally induced residual stress is generated by nonuniform heating and cooling operations during welding, which results in constraint on thermal expansion and contraction. At a microscopic level, a mismatch between coefficients of thermal expansion and coherency of the crystallographic structures of the neighboring phases will contribute to the development of thermally induced residual stress [22]. A global "shrink-fit" effect occurs between the clad and substrate materials, influenced by the material and temperature dissimilarity [23,24]. Chemically generated residual stresses can develop because of volume changes associated with chemical reactions, phase transformation and microstructural evolution, such as precipitation hardening [22]. Often, such factors are observed through their influence on material properties and, ultimately, the resulting nature of the residual stresses [14,25]. Lastly, the spatial and temporal variation of the clad deposition process and subsequent cooling rate of the component also contributes to the residual stress state [26]. Variation in the temperature of clad and substrate materials affects cooling rates and, in turn, constraint levels in the component. Material properties vary with temperature and time; therefore, the thermal transient process that arises is heavily dependent on the differing expansion and contraction rates. During cooling, yield strength and Young's modulus develop with values differing in neighboring regions, hence the resulting variation in thermal stress [27–29].

Improvement in fatigue life is often investigated by examining the residual stress state and the benefit of methods that alter the residual stress state. However, many investigations into the welding or cladding of superalloy IN625 focus on microstructural evolution, material properties, and often corrosion resistance [18,30–37]. This is of particular interest in the region where operational stresses are highest, commonly at the surface of a component or structure. Upon superimposing residual and operational stresses, ideally the entire stress cycle would remain in the compressive range. However, any level of compressive residual stress would be beneficial in lowering the combined stress level. An in-depth understanding of the effects of the welding process on the residual stress state, material properties, and fatigue performance of the component is required and is what forms the basis of this research.

In this study, a low-alloy 4330 carbon steel weld clad with a IN625 nickel-based superalloy has been investigated to deduce the magnitude and distribution of the residual stress induced by the cladding process. This includes surface, near-surface, and bulk

residual stress throughout the clad layer to the base material, which were measured using different techniques. These techniques include X-ray Diffraction (XRD), hole drilling based on electronic speckle pattern interferometry (ESPI), deep-hole drilling (DHD), and the contour method (CM). A variety of residual stress measurement techniques are well presented by Kandil et al. [7], who highlighted practical, material, and physical considerations as well as the advantages and disadvantages of the techniques. These methods are complementary and therefore a measurement program such as that presented herein must gain an accurate understanding of the residual stress distribution throughout a component. Comparisons have been made between the results of XRD and ESPI for surface residual stresses and DHD and CM for through-thickness residual stresses.

## Experimental Procedure

### MATERIAL AND PROCESSING

The material chosen for this investigation was a low-alloy 4330 carbon steel in the form of a hollow cylinder. A schematic representation of the specimen, dimension labels, and measurement locations are shown in **Fig. 1**, and measured values are presented in **Table 1**. Weld overlay cladding of the cylinder was achieved using hot-wire GTAW to deposit a layer of IN625 onto the outer diameter of the hollow steel cylinder. The outer diameter was selected for deposition of the clad layer as it was deemed that the nature of residual stresses would be similar on both the inner and outer diameters because the cylinder thickness was greater than the clad layer thickness. This thereby facilitated simpler deposition of the clad material and allowed for residual stress measurements using a variety of techniques; both aspects would have experiencing increased complexity and limitations had the clad layer been deposited on the bore. The weld cladding process created a bond between the base and the cladding material, with a periodicity of one bead per 3.40 mm. Each bead is composed of approximately two small weld ripple pockets per 4.74 mm,

**FIG. 1**

(a) Schematic representation of the weld clad cylinder detailing dimensions of interest, plane of cut for the contour method, measurement locations for XRD and ESPI, and stress orientations (A and H being axial and hoop stresses, respectively). (b) Illustration of weld surface with position of XRD (red circle) and ESPI (dashed circle) measurements showing a magnified image of the position of a drilled hole to indicate the scale with respect to the weld bead, along with a schematic representation of the weld peaks and troughs.
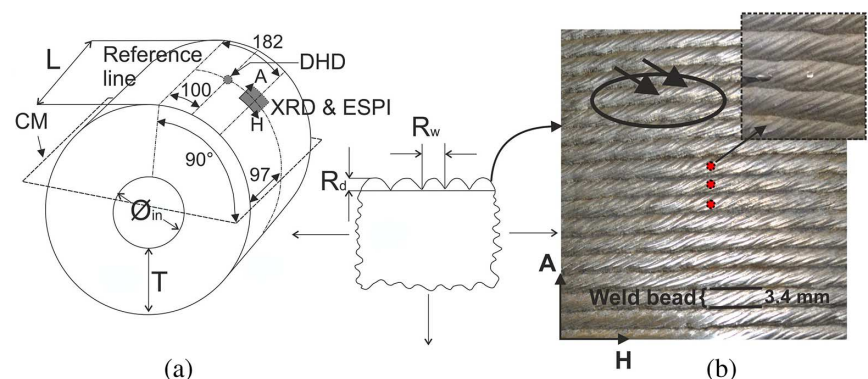
**TABLE 1**

Weld clad specimen dimensions.

| Variable | Label | Measured Value (mm) |
|---|---|---|
| Inner diameter | $\varnothing_{in}$ | 126.80 |
| Cylinder length | $L$ | 193.32 |
| Wall thickness | $T$ | 100.16 |
| Bead depth | $R_d$ | 0.35 |
| Bead width | $R_w$ | 3.40 |
| Clad layer thickness | | 6 |

**TABLE 2**

Typical nominal chemical composition of 4330 alloy steel and superalloy IN625 welding wire.

| 4330 | | IN625 | |
|---|---|---|---|
| Fe | 95.3–98.1 % | Ni | 58 % min. |
| Ni | 1–1.5 % | Cr | 20–23 % |
| Mn | ≤1 % | Mo | 8–10 % |
| Si | ≤0.8 % | Nb+Ta | 3.15–4.15 % |
| Cr | 0.4–0.6 % | Fe | 5 % max |
| Mo | 0.3–0.5 % | Al | 0.4 % max |
| C | 0.2–0.3 % | Ti | 0.4 % max |
| | | C | 0.1 % max |
| | | Mn | 0.5 % max |
| | | Si | 0.5 % max |
| | | Cu | 0.5 % max |
| | | P | 0.015 % max |
| | | S | 0.015 % max |

oriented within 161.46 ± 6.56° of the specimen's radial direction (see **Fig. 1b**). A two-pass deposition process was utilized, resulting in a total clad layer thickness of 6 mm. The nominal chemical composition of substrate and clad materials are summarized in **Table 2**. A single cylinder was utilized for all residual stress measurements that will be presented in the following section. Measurement locations were selected in consideration of the accuracy of measurements; for example, the surface utilized for deep-hole drilling was an intact surface as opposed to the location at which a hole had been drilled for a hole drilling measurement.

**RESIDUAL STRESS MEASUREMENT**

**XRD**

Surface residual stress measurements were obtained using XRD, in which a PROTO-LXRD diffractometer (Proto, New Britain, CT) and the $\sin^2\psi$ method [38] were utilized. Stresses were calculated from the strains of the {311} Bragg reflection, assuming elastic Young's modulus of $E = 168$ GPa, according to the experimental measurement of this property in the clad layer, and Poisson's ratio of $\nu = 0.29$. A Mn K-α target tube with a wavelength of 2.1031 Å was utilized. Measurements were obtained at psi offset angles of 0°, ±4.36°, ±13.6°, ±18.69°, ±24.48°, and ±30°, with a ±3° oscillation at each angle and an angle of ±13.6° between the beam and each detector. Measurements were undertaken using a 2-mm round collimator, as highlighted in **Fig. 2**, in two perpendicular directions: axial,

**FIG. 2** (a) Orientation of $\varphi$-angles during XRD stress measurements with respect to the global component axes, (b) local weld beads and the arrangement of weld ripples within each bead, and (c) relation of weld bead geometry to the incident X-ray aperture.
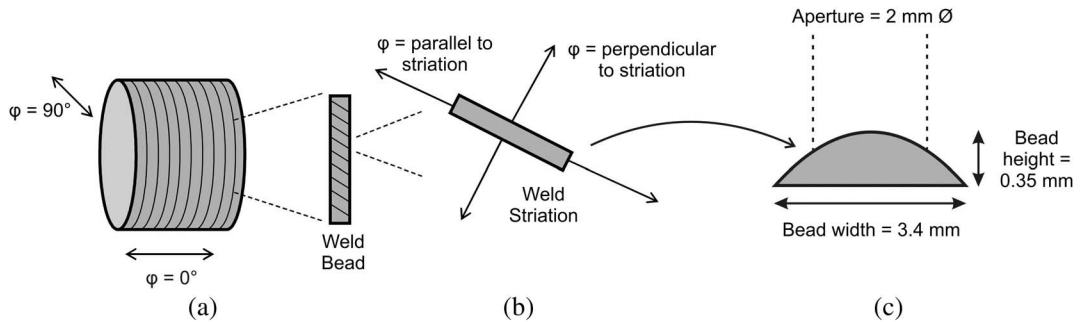


along the length of the cylinder ($\varphi = 0°$) and hoop, tangential to the surface of the cylinder ($\varphi = 90°$). Two extra measurements were also performed at $\varphi = 60°$ and $\varphi = -23°$ to represent the directions parallel and perpendicular, respectively, to a striation (i.e., weld ripple pockets) in the weld bead. These angles are schematically illustrated in **Fig. 2b**. It should be noted that because of the irregularity of the weld clad deposition, care was exercised to ensure the most appropriate definition of the directions that were parallel and perpendicular to the striation; thus, these values depend on measurement location and cannot merely be considered as mathematically perpendicular, i.e., at 90°, to one another. Consideration of the beam diameter ensured that all measurements were obtained solely across one weld bead; however, curvature of the weld bead was unavoidable, as illustrated in **Fig. 2c**.

Measurements were obtained in each case along a path consisting of 20 adjacent weld bead peaks from the reference face of the specimen. The assigned point numbers reflect the weld bead peak, which are numbered from the reference edge.

### Hole Drilling Based on ESPI

A Stresstech Prism system (Stresstech Oy, Jyväskylä, Finland) was used to measure residual stress using the hole-drilling method based on ESPI [39]. The Prism system consists of a high-speed drill, laser source, and a charge-coupled device (CCD) camera. A coherent laser source illuminates the specimen surface and interferes with a separate laser beam originating from the same source as the reference beam to form a speckle pattern. The low reflectivity of the as-clad surface provided an ideal surface for drilling. Drill diameters determine the depth to which measurements can be obtained, i.e., residual stresses obtained to a depth of 60 % of the hole size. A drill diameter of 1.8 mm was utilized in this case, ensuring that measurements were not obtained across more than one weld bead. The drill was centered on top of the weld bead in the central weld bead at various locations in the region highlighted in **Fig. 1b**, drilling on the as-clad surface to obtain a quality hole. Residual stresses were calculated from the strains measured by ESPI during incremental drilling, assuming the mechanical properties noted in **Table 3** for the clad material (i.e., superallot IN625).

### DHD

DHD measures strain relief through the drilling of a reference hole and an electrodischarge machine (EDM) trepanned core comparing differing diameters due to mechanical

**TABLE 3**

Mechanical properties for clad and substrate materials, obtained experimentally.

| Material | Yield Strength (MPa) | Young's Modulus (GPa) | Poisson's Ratio |
|---|---|---|---|
| IN625 | 474 | 168 | 0.29 |
| 4330 | 869 | 189.8 | 0.289 |

relaxation. Converting measured strains and using elastic theory, residual stresses were obtained through the thickness of the component. The trepanning of the hole during measurement caused the release of residual stress in the vicinity of the trepanned region, and the displacement $[\delta]$ was described in relation to the original stress through the following equation [40]:

$$[\delta] = -\frac{1}{E}[D][\sigma]$$ (1)

In this equation, $E$ is the Young's modulus and $[D]$ is a matrix relating to the hole edge displacement in a stressed plate; the theory of DHD has been well described in various studies [41–43].

DHD was performed using a reference hole drilled in the cylinder's radial direction from the clad surface to the bore. The reference hole was located halfway along the cylinder's axis. This enabled the measurement of the axial, circumferential, and axial-circumferential shear components of the residual stress at the reference hole location as a function of through-wall depth. The reference hole had a nominal diameter of 3 mm and, using a coaxial EDM trepan with a diameter of 10 mm, was incrementally relieved of stress.

Measurement of the reference hole was performed at trepanning increments of 2.5 mm up to a depth of 20 mm, and again after trepanning to the full depth of the hole. In each measurement, the reference hole diameter was determined with an air probe at angular increments of 22.5° every 0.2 mm between the clad surface and the pipe bore. Residual stresses were calculated from measured diametral displacements using Eq 1. In this calculation, differing elastic properties were used for the IN625 superalloy cladding material and the 4330 carbon steel cylinder wall material, as given in **Table 3**. Results from the incremental trepanning steps indicated that no significant plasticity occurred close to the reference hole during the measurement, so the incremental analysis procedure described by Mahmoudi et al. [42] was not required.

## Contour Method

The contour method provides a 2-D map of out-of-plane residual stress in the cut direction using Bueckner's superposition principal to section the component [44]. The first cut in the axial plane, as shown in **Fig. 3**, provides the hoop residual stress, and the second cut in the hoop plane provides the axial residual stress.

The contour method was carried out on the clad cylinder to provide a full 2-D map of both hoop and axial residual stress distributions in the sample. For the hoop residual stress, the contour method included the release of bending moments, as described by Prime [45], which acted as an additional source of hoop residual stress. The measurement of each stress component was carried out in four main steps of sample cut: measurement of cut surface profiles, data processing, and calculation of residual stress using finite element simulation.

**FIG. 3** Cutting directions to obtain (a) hoop and (b) axial stress components, figures indicating orientations of all stress components.



(a)

(b)
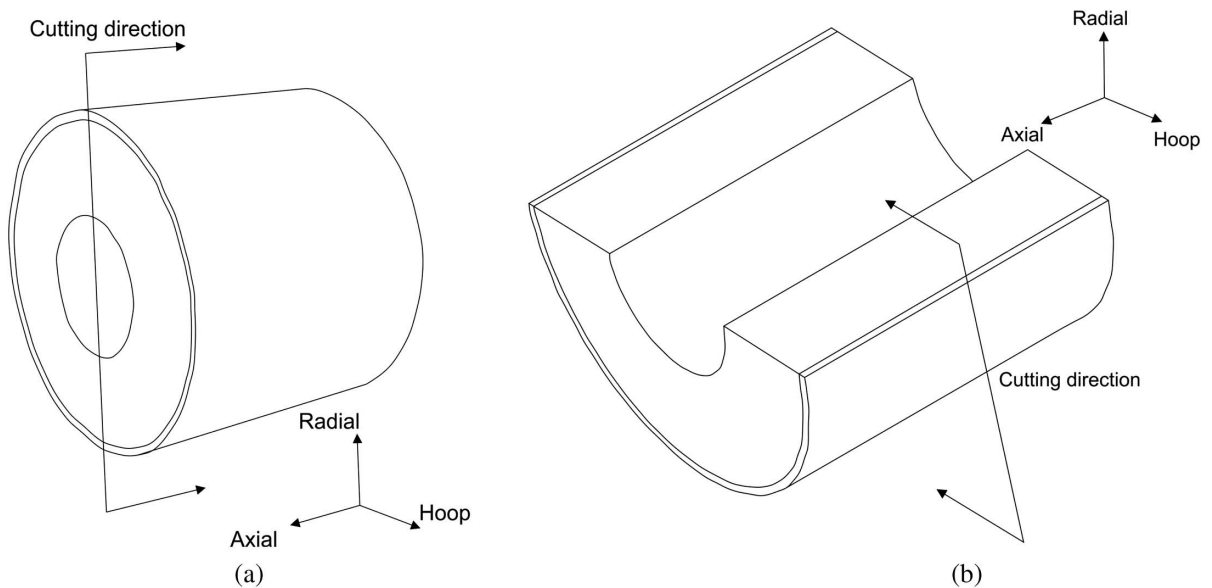
EDM wire entry and exit from the test specimen can introduce cutting artifacts that affect near-surface measurements. Wire entry refers to the top face of the specimen where the running wire enters the test specimen. Wire exit relates to the bottom face of the specimen where the running wire leaves the test specimen. To mitigate the cutting artifacts from wire entry and exit, sacrificial layers were bonded on the top and bottom faces of the pipe and the bore in the vicinity of the cut plane [46]. The cuts were made by EDM using a 250-μm brass wire in "skim" cut mode. For the hoop stress component, the cut was made in the axial direction on the axial-radial plane (**Fig. 3a**) covering the entire part, starting from one end to the other. Prior to sectioning, two pilot holes with 3-mm diameters were drilled approximately 5 mm from both ends of the pipe, such that the cut was conducted from the center of a hole on one side to the center of the hole on the other side of the part, aiming to cut the test specimen using an embedded cutting configuration. The advantage of this technique is that it provides self-constraint, which restricts opening of the cut faces and thereby controls the stress concentration and reduces the risk of significant plasticity arising at the cut tip during cutting. Following the completion of the cut, the remaining ligaments were severed to separate both halves of the part.

A single contour cut [47] was used to determine the distribution of hoop stresses on an axial-radial plane, bisecting the clad pipe, that is, simultaneously mapping the hoop stresses on two wall thicknesses that were 180° apart. Moreover, the measured stress field included the effect of hoop bending stresses and their variation along the pipe. This approach has several advantages over the Prime approach [45]: a single cut is required (instead of three cuts), stresses in diametrically opposite sides of the pipe are determined (compared with stresses on a single side), and any variation in hoop bending stress, if present, along the length of the pipe is captured.

For the axial stress component, the contour method residual stress measurement was conducted on one half of the part, as shown in **Fig. 3b**. Again, sacrificial materials were

bonded to the inner and outer diameters to create a uniform cross section. Because the contour method measurement on one half can only provide a partial axial residual stress component, the total axial stress is obtained through the principal of superposition, as expressed in Eq 2:

$$\sigma_{\text{Axial, total}} = \sigma_{\text{Axial, relaxed}} + \sigma_{\text{Axial, remaining}} \qquad (2)$$

where the relaxed axial stress arises because of the first cut undertaken to measure the hoop stress, and the remaining axial stress was due to the second contour cut [48,49].

Upon completion of the EDM cuts, the outline and surface topography were measured for each cut on either side of the skim cut in a temperature-controlled environment using a laser hybrid coordinate measuring machine (CMM). The CMM equipment was programmed to acquire data with a spatial resolution of 100 µm for points in both in-plane directions.

The measured data obtained for both surfaces of each skim cut were aligned in the same coordinate system by considering the whole perimeter of each half of the cut as an alignment guide to match the outlines. Following the alignment process, the datasets for both sides were linearly interpolated onto a common grid, after which the two sets were averaged. Noise and outliers in the averaged dataset were then removed before smoothing the data. A knot spacing of 1 mm$^2$ was selected for the calculation of hoop and axial stress, and a bivariate cubic spline for each knot spacing was fitted to the averaged data.

A 3-D finite element model assuming isotropic elasticity, with a Young's modulus of 168 and 189.8 GPa and a Poisson's ratio of 0.29 and 0.289 for the clad and substrate materials, respectively, was used to evaluate the residual stress from the surface contour data. For this purpose, the perimeter of the cross section for each sample was modeled using the aligned outline measured by the CMM. The 2-D cross section was then rotated circumferentially by 180° for the hoop stress component and extruded to the length of the cylinder, which was 250 mm, for the axial stress component, producing 3-D models for the calculations of residual stress. Mesh seeds were attributed to each node on the outline and along the revolved and extruded perimeters of the models that are used as guidelines for the generation of mesh. The establishment of the seeds were biased by allocating a finer pitch near the cross section of the model that represents the cut surface and a coarser pitch toward the other end of the model, the latter of which being of less importance for stress analysis. The parts were modeled in Abaqus CAE (Dassault Systèmes, Vélizy-Vilacoublay, France) and meshed with a fine mesh of 0.4 mm in the clad layer and 4 mm toward the inner diameter. For the residual stress model, the stresses were calculated by forcing the cut surface into the opposite shape of the averaged contour data [19,50,51].

## Results

### XRD

FIG. 4 illustrates the presence of variations in measured residual stress magnitudes in both the axial and hoop stress components on the as-clad surface, wherein the majority of measurements and the average values are compressive in nature. The uncertainty for each measurement point is evaluated based on the best fit to the sin$^2\psi$ method. The average values are calculated by averaging the stresses measured for all points, and their associated uncertainties were calculated by taking the second root of the sum of the squares of the uncertainties of all points evaluated by the sin$^2\psi$ method.

**FIG. 4** (a) Axial and (b) hoop residual stresses measured on 20 consecutive weld bead peaks in IN625 as-clad surface using XRD.



(a)                      (b)
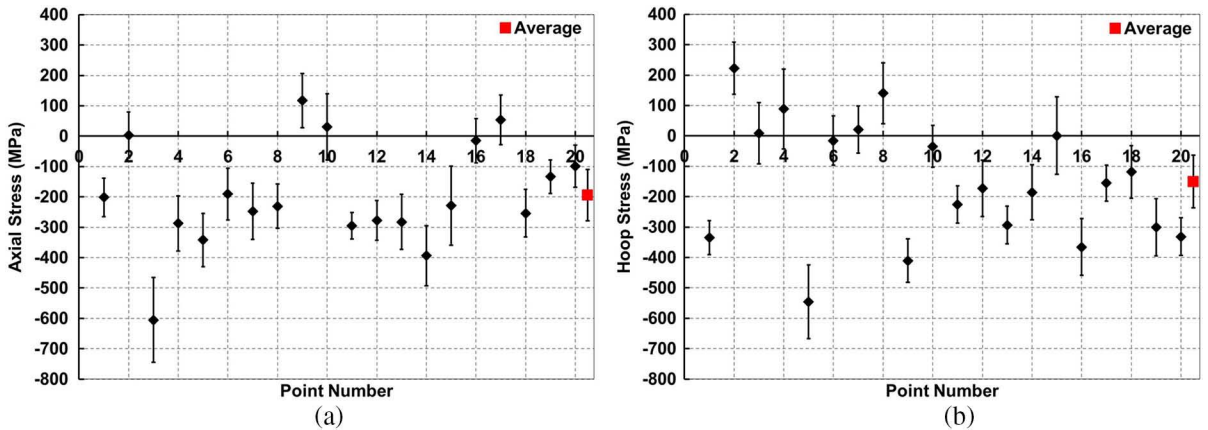
## HOLE DRILLING BASED ON ESPI

The depth profiles of the residual stress distribution quantified by hole drilling based on ESPI for different weld beads are provided in **Fig. 5** and display the data obtained for both hoop and axial directions. The measured hoop and axial components indicate the presence of compressive residual stress with a maximum of −390 and −511 MPa, respectively, on the surface. These were then reduced to a stress-free state in both directions at a depth of approximately 0.3–0.5 mm in most cases, at which point the nature of stress tended to transform to tensile. Both hoop and axial stress components increased in a tensile manner deeper into the clad layer, to a maximum of +233 MPa and +407 MPa at a depth of 1.2 mm, respectively. Given that the 1.8-mm drill diameter was utilized, residual stress was measured to a depth of 1.2 mm. Offset depths are utilized here, indicating the beginning of a measurement at an effectively zero depth by the removal of material to reveal a complete circle. However, clearly for the means of comparison with other methods, the depth from the clad surface will be used in later comparisons.
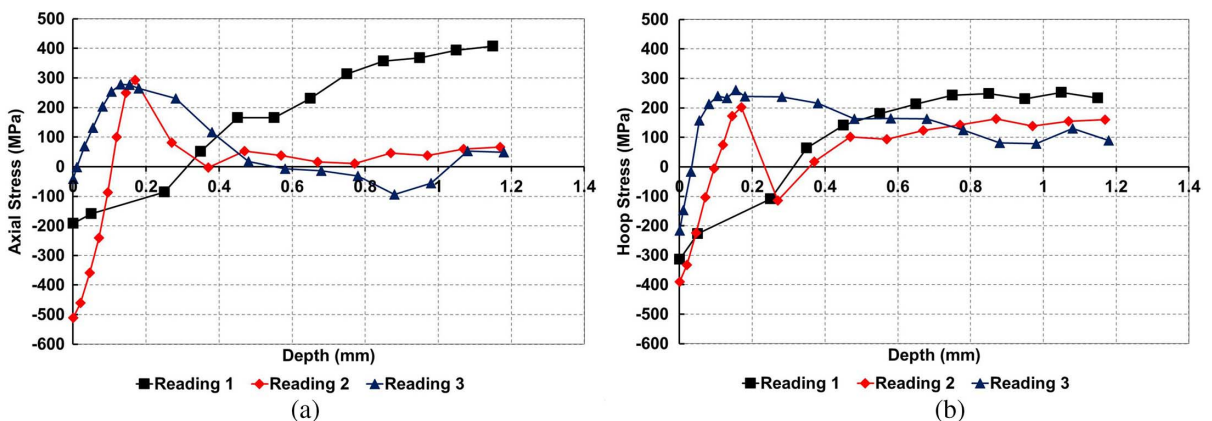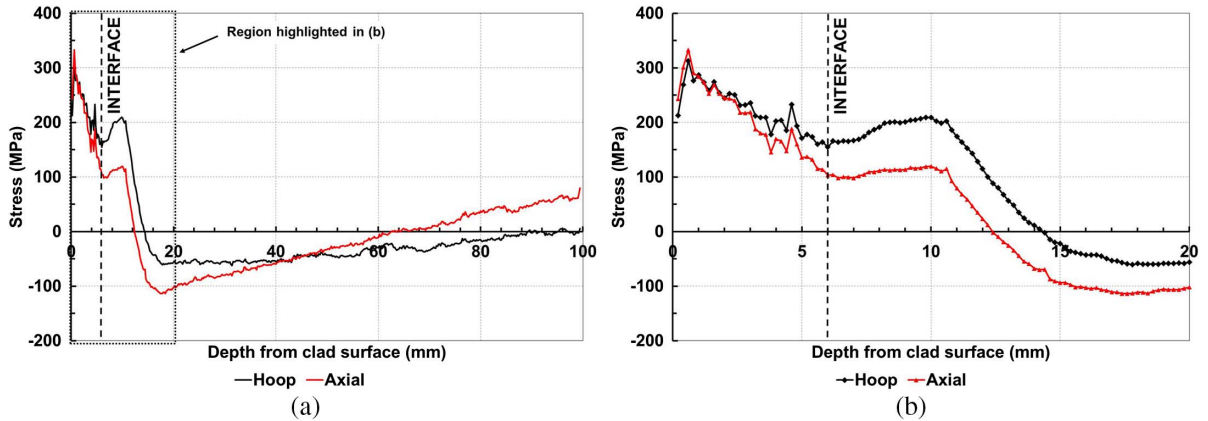
**FIG. 5** (a) Axial and (b) hoop residual stresses measured on weld bead peaks in IN625 as-clad surface using ESPI.



(a)                      (b)

**FIG. 6** Hoop and axial residual stresses (a) throughout cylinder (b) in region of clad; heat-affected zone (HAZ) and substrate measured in IN625-clad cylinder using DHD.



(a)                    (b)

## DHD

**Fig. 6a** illustrates the hoop and axial residual stresses throughout the section, which indicates that the general trend and nature of residual stress are similar for both components. Tensile residual stresses with magnitudes of +212 ± 20 MPa and +243 ± 20 MPa are present on the surface for hoop and axial components, respectively, which reduces to 0 MPa at a depth of 12–15 mm, depending on the direction. Because of the self-equilibrating nature of residual stress, compressive stresses are measured further into the substrate, counterbalancing the tensile stresses on the surface.

**Fig. 6b** presents the results that concentrate on the vicinity of the joint between clad and substrate materials. Beyond a depth of 5 mm, a smoother profile emerges, illustrating the change between clad and substrate materials. At the interface, there is no sharp discontinuity present, as was illustrated in the previous modeling results [52]. Such discontinuity stresses were expected to be exaggerated because of the idealized interface modeled, which did not account for alloying and diffusion due to the weld cladding process [53]. A slight increase in tensile residual stress occurs immediately upon entering the substrate material, prior to a decrease into the compressive region. Small levels of compressive residual stress between 15–20 mm exist on the outer diameter, which indicates that alloying and diffusion successfully smooth potential stress discontinuities that are due to dissimilar materials.

## CONTOUR METHOD

**Figs. 7** and **8** show the contour plots of the averaged surface height that were obtained by the CMM following the EDM skim cut for both hoop and axial stress measurements, respectively. The contour range of peak to valley exceeds 120 μm for the hoop component and 45 μm for the axial component. The contour plots show that the surface height for both directions is low in the weld region, which implies that tensile residual stresses are relieved.

The contour plot of the out-of-plane hoop residual stress measured on the sectioned surface is shown in **Fig. 9**. This plot illustrates a consistent pattern from the clad surface into the substrate to the bore. From the hoop stress map provided in **Fig. 9**, it can be seen that

**FIG. 7**

Contour plot of the averaged surface height in millimeters obtained by the CMM for the hoop stress measurement.
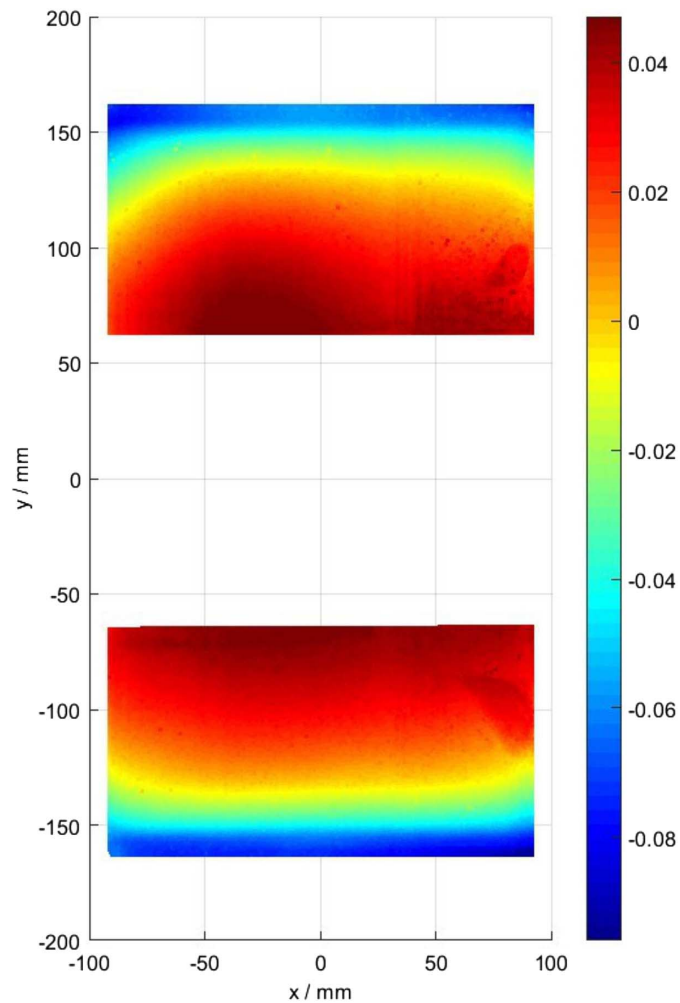


tensile residual stresses (i.e., green to red) were largely concentrated within the clad layer and the heat-affected zones (HAZ) in the interference zone between the clad and the substrate. Hoop residual stress profiles are presented in **Fig. 10**, and six chosen paths are highlighted in **Fig. 9**, emphasizing the clad layer and the substrate interface in **Fig. 10b**. The region of highest tensile residual stress was identified immediately at the clad surface with a peak stress reaching +677 MPa, as shown in the data for Path 1 in **Fig. 10b**.

**Fig. 10a** shows a high-tensile residual stress at the clad layer surface followed by a decrease to a notable compressive residual stress. An increase to tensile residual stress remains at a depth of around 15 mm, with compressive residual stresses similar to those measured by DHD, then emerges in the substrate.

Focusing on a region in the vicinity of the join, as shown in **Fig. 10b**, the data shows compressive residual stress at a depth of 2 mm ranging between −316 and +72 MPa for the various paths. Such variations are thought to be due to the spatial weld cladding process and weld bead peak and trough effects, thus resulting in varying residual stress

**FIG. 8** Contour plot of the averaged surface height in millimeters obtained by the CMM for the axial stress measurement.
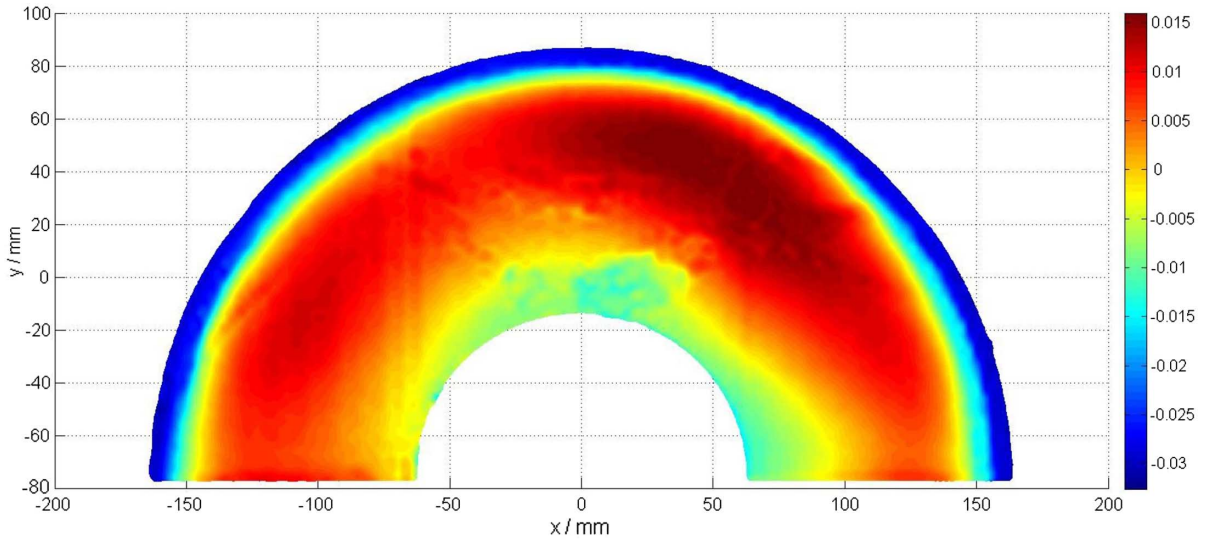


**FIG. 9**

Hoop residual stress (MPa) measured in the IN625-clad cylinder using CM, illustrating paths utilized in **Fig. 10**.
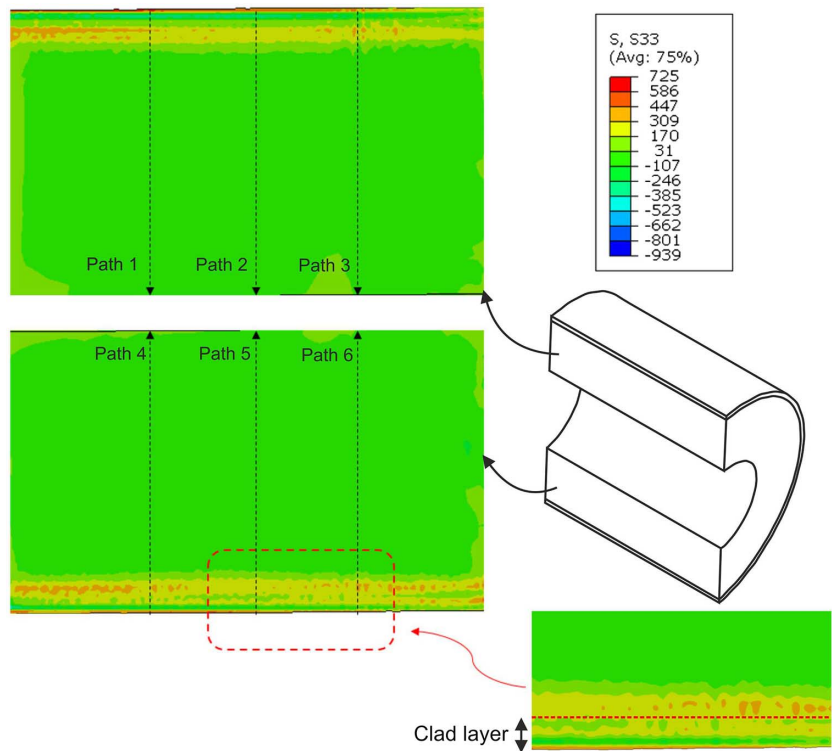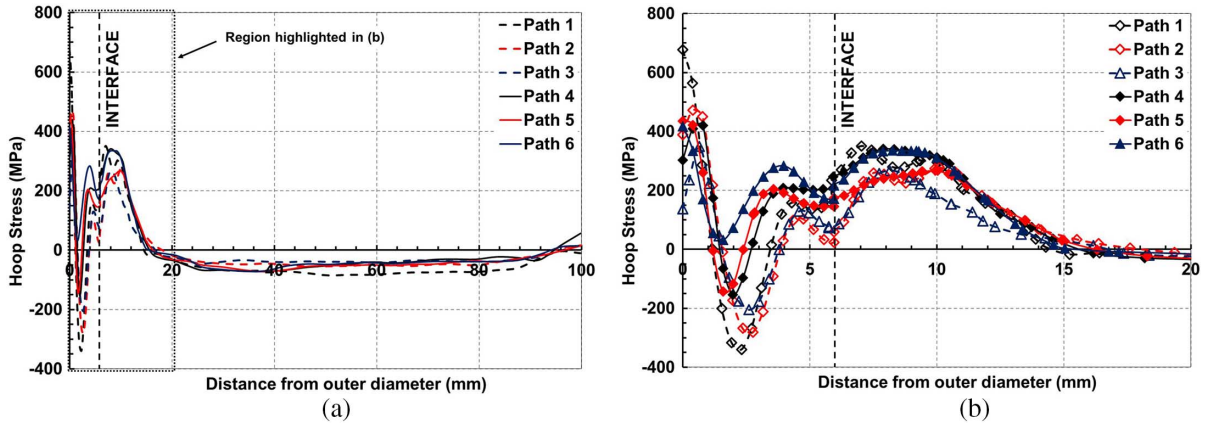
**FIG. 10** Hoop residual stress profile (a) throughout the component and (b) in a region of clad layer and HAZ in IN625-clad cylinder using CM plotted along six paths, as illustrated in **Fig. 9**.



(a)

(b)

distributions along the length of the cylinder, as highlighted in **Fig. 9**. It should also be noted that the various methods utilized herein have varying degrees of spatial resolution, and the spatial resolution requirements should always be considered during technique selection [7,54]. In this study, it is highlighted that it was only through the complementary use of XRD, ESPI, DHD, and CM that a detailed residual stress distribution could obtained both in the weld clad layer and throughout the component.

Axial residual stresses superimposed for the relaxed stresses of the first cut and the remaining measured stresses of the second cut produce the stress map shown in **Fig. 11**. The plots of the three lines in **Fig. 11** indicate (see **Fig. 12**) that the axial stress possesses a much smoother nature than the hoop stress component, with a consistent tensile residual stress in the clad layer continuing into the substrate. Compressive axial stress is measured in the substrate to a similar level as that measured by DHD.

**FIG. 11**

Total axial residual stress (MPa) measured in the IN625-clad cylinder using CM, illustrating paths utilized in **Fig. 12**.
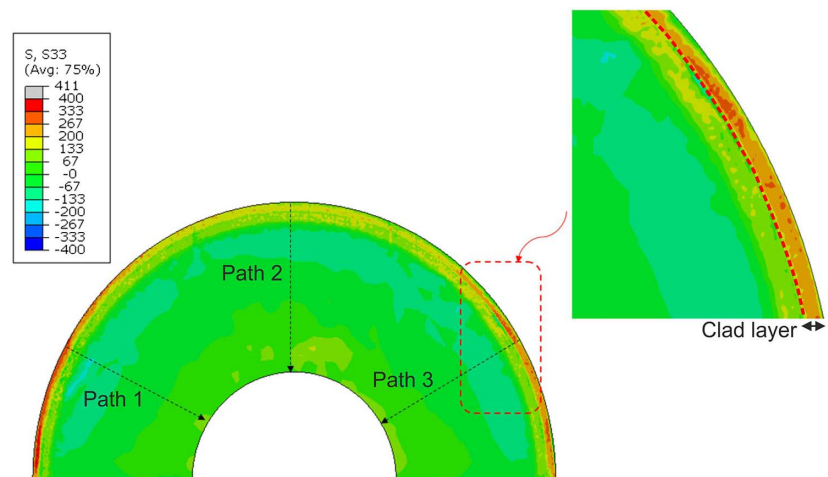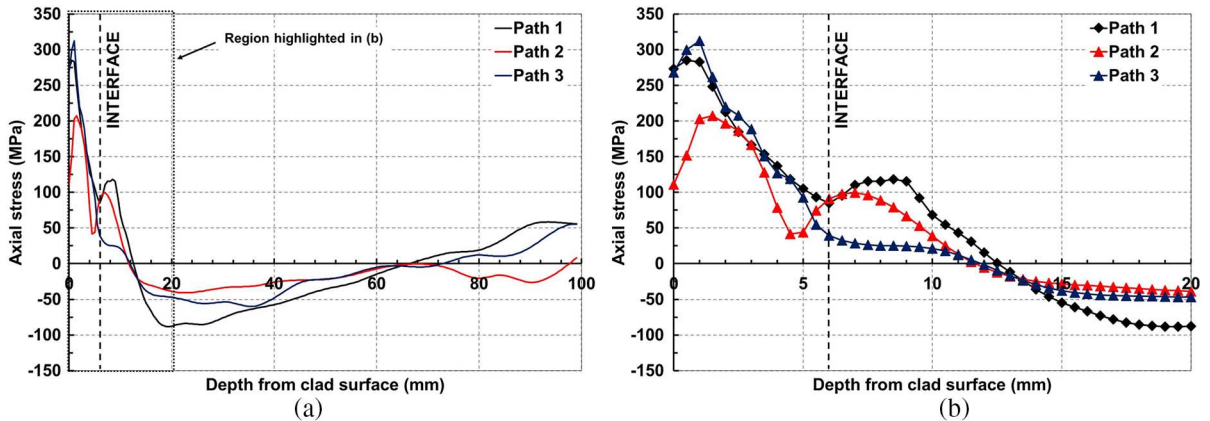
**FIG. 12** Axial residual stress profiles (a) throughout the component, and (b) in a region of clad layer and HAZ in the IN625-clad cylinder, measured using CM along the three paths illustrated in **Fig. 11**.



(a)

(b)

## Discussion

The following section presents a comparison of results that were obtained using all the aforementioned measurement techniques along with a discussion of the considerations related to the obtained residual stress distributions.

### COMPARISON OF SURFACE AND NEAR-SURFACE RESIDUAL STRESS

Surface and near-surface residual stresses were measured using the XRD and hole-drilling methods based on ESPI, respectively. The penetration depth of the X-ray used in these measurements was approximately 10 μm in the IN625 superalloy, while the ESPI measurements were obtained incrementally at a depth of 20–50 μm from the surface to a depth that was dependent on the level of material removed to reveal a complete circle. Therefore, these methods are complementary in constructing the residual stress profile in the surface region.

XRD measurements obtained on weld bead peaks did not provide wholly consistent results, as shown in **Fig. 4**. This may be due to a slight difference in the positioning of the X-ray beam on the weld bead and variation in the number and morphology of the weld ripple pockets (i.e., striations) covered by the beam. If the beam is not perpendicular to the peak of the weld bead, then stress values may vary significantly [38]. Axial and hoop stress values appear to have been potentially influenced by these factors. **Fig. 4b** suggests that, toward the edge of the cylinder, hoop stresses are generally tensile, while cylinder compressive stresses are measured further from the edge. However, this does not appear to be the case for axial stresses, as shown in **Fig. 4a**, which are largely compressive regardless of distance from the reference face. The error is calculated as a best fit to the $\sin^2\psi$ method and hence larger error values may manifest because of striation effects, surface irregularities, large grain sizes, and texture. Error values also differ greatly between point measurements, which is likely due to the curvature [38] of the weld bead if deviation from a perpendicular beam to surface condition occurs. The X-ray beam did not extend across more than one weld bead; however, the beam may deviate from normal to the weld bead, depending on the measurement surface (i.e., the curved bead).

Strain values are averaged across the measurement region, thus calculated stress values are also affected. Geometrical variations and surface irregularities could also lead to inaccuracies in stress values [38]. The surface profile and weld bead geometry will vary across the cylinder, potentially affecting stress values. As highlighted in **Fig. 4**, the majority of axial and hoop residual stress values, along with average values obtained using XRD on the weld bead peaks, were compressive. Inconsistencies in the measurements obtained using XRD alone prove the difficulty in comparing residual stress measurement methods. However, this is not due to an inaccuracy of the measurement technique but because the technique is identifying varying levels of residual stress due to the weld bead geometry.

ESPI also indicated compressive residual stresses immediately at the clad layer surface (i.e., near-surface residual stress). These compressive residual stresses were similar in magnitude (i.e., within 3 MPa of the axial stress component and 166 MPa in the best-case comparison) to those obtained using XRD. ESPI then showed a transformation into tensile residual stress in both hoop and axial stress components at a depth of 0.3 mm, after which the level of tensile stress increased to +233 and +407 MPa at the furthest depth of measurement obtained. The presence of compressive residual stresses on the surface and near-surface is a characteristic of fast-cooling from elevated temperatures that happens immediately after the weld is embedded. The high heat exchange rate between the hot surface and the environment leads to a differential contraction and expansion between a cold surface and hot interior at the early stages of cooling that can plastically deform the surface [8]. Subsequently, when the entire part has cooled to room temperature, the plastically deformed surface is forced by the bulk interior material to a location and condition that generates compressive residual stress [12]. Because of the self-equilibrating nature of residual stress, an area immediately below the plastically deformed surface develops tensile stress to counterbalance the compressive stress on the surface. This phenomenon has been seen in this study, as shown in **Figs. 13b** and **14b**. The presence of a compressive residual stress is particularly beneficial at the surface of a component where operational stresses are often highest. Upon super-positioning of the residual stresses with cyclic operational stresses, the entire stress cycle would ideally remain in the compressive region and, in turn, crack propagation would tend not to occur [5,25,55,56]. Crack

**FIG. 13** Comparison of axial stress measured (a) throughout component and (b) in the region of clad layer and HAZ in IN625-clad cylinder using XRD, ESPI, DHD, and CM.
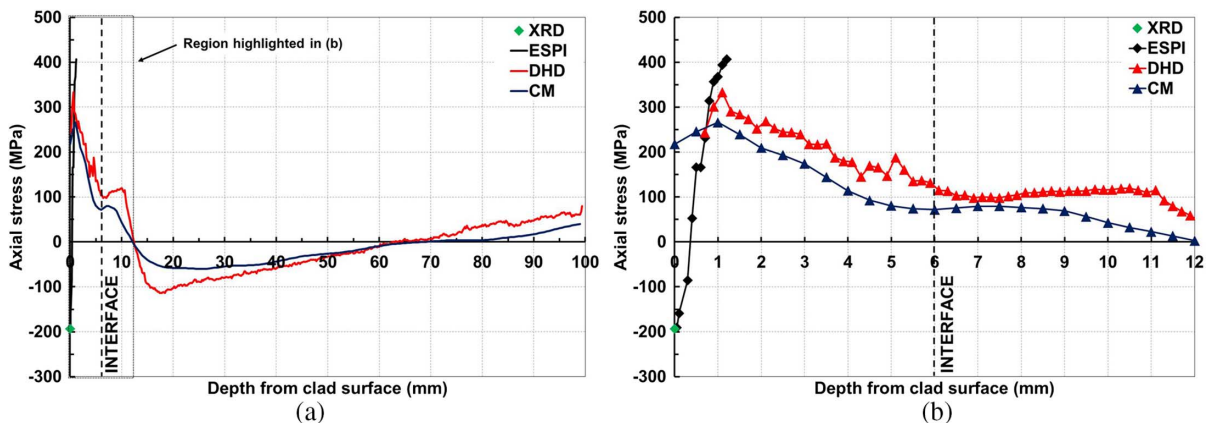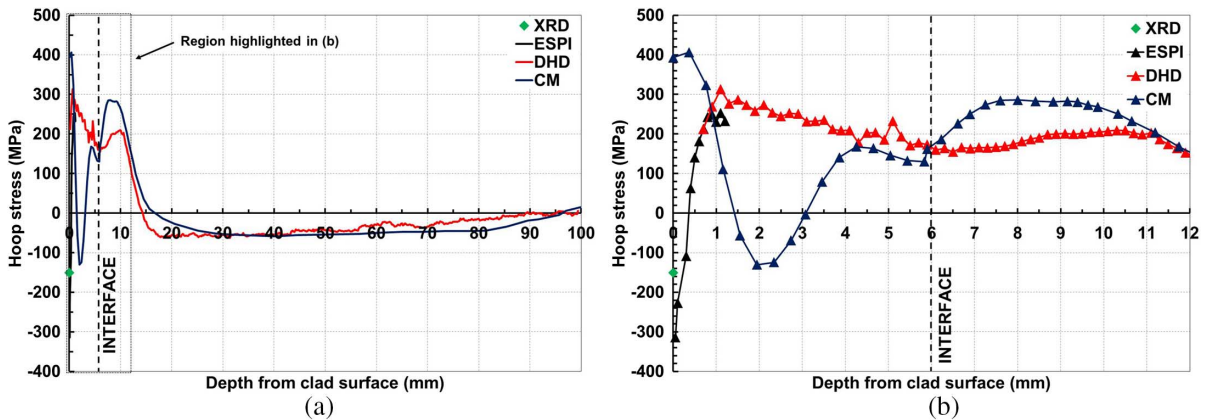
Comparison of hoop stress measured (a) throughout component and (b) in the region of the clad layer and HAZ in IN625-clad cylinder using XRD, ESPI, DHD, and CM.



(a)          (b)

initiation is, however, thought to be uninfluenced by the presence of compressive residual stress [42] or can be enhanced by Type III residual stress [57]. Compressive residual stress can also improve corrosion performance and stress corrosion cracking performance for some materials [30,57,58].

## COMPARISON OF THROUGH-THICKNESS RESIDUAL STRESS

The compressive residual stresses obtained directly on the surface using XRD and ESPI are complementary to the data measured by DHD and the CM to reconstruct the full stress profile from the surface through the clad layer and into the bulk material. Both DHD and CM techniques measured tensile residual stress close to the surface, in reasonable proximity to the data obtained by ESPI. The air probe used in the DHD method cannot measure accurately at depths of less than ≈1 mm from the surface, leading to the loss of stress information at the surface and near-surface. This information is measured by the XRD- and ESPI-based hole drilling (see **Figs. 13** and **14**). The data shows that different measurement techniques can detect variations in residual stress but not to the same resolution despite all considering for the measurement of Type I residual stress. This is the greatest differentiating factor between the surface, near-surface, and through-section measurement techniques. Clearly, the results are also location dependent and, as such, the discrepancies that arise in comparative figures are to be expected given that locations differ. It is further noted that in the CM results, as has been illustrated, the level of residual stress measured at the surface and into the clad layer is dependent on the path through which stresses are plotted. This can be due to slight variations in the residual stress distribution in the axial direction, or perhaps because of the weld cladding process or consequent cooling; although, CM can also struggle to provide details of residual stress close to the edges should cutting artifacts be present [46].

In comparing DHD and CM results, residual stress deeper in the component can be evaluated. Axial and hoop residual stresses are shown for both methods in **Figs. 13** and **14**, respectively. The data plotted for the contour method is the average for both axial and hoop stresses (**Figs. 12** and **10**). Comparing these results illustrates that the stress distributions obtained are comparable in general, with large tensile residual stresses close to the

clad layer surface that tend to decrease toward the interface. Compressive residual stresses are observed in the substrate for both measurement techniques and both stress components, prior to a transformation into tensile residual stresses at the cylinder bore. At a depth of 2 mm in the hoop component, there is a discrepancy with stress levels in the CM results, decreasing into the compressive region, highlighted clearly in Fig. 14b. Even though decreasing the knot spacing increased accuracy in such regions, the noise in the measurement increased. Therefore, care must be taken when selecting the parameters for calculation of the residual stress to ensure that sufficient detail is obtained while minimizing data noise [59]. Stress values obtained using DHD are supported by those of ESPI with tensile residual stresses of +274 MPa obtained at a depth of 1.2 mm compared with +233 MPa obtained using ESPI. When the stress level of CM data reached a high tensile residual stress once more, the data for DHD and CM was similar.

Comparing the residual stresses measured on the surface, near-surface, and through-thickness, it is clear there are surface effects due to the geometry of the weld bead that influence the residual stress immediately at the surface that cannot be measured by both DHD and CM. This is because DHD requires surface preparation that results in the elimination of surface and near-surface stress data, while CM results may be subject to cutting artifacts. Furthermore, surface irregularities caused by the weld bead peaks and troughs along with weld pass effects present complexities in evaluating the residual stress with high sensitivity such that these cannot be precisely measured by the laser CMM. This, in turn, increases the uncertainty associated with the finite element simulation and application of the superimposition principle of the contour method. The average peak to trough measurement was 0.35 mm, as noted in Table 1, and was not considered in the contour method measurement. Thus, the weld surface edge in Fig. 9 appears as a straight line whereas in reality it is a "serrated" edge, as shown in Fig. 1. Various studies have shown that the weld bead geometry and behavior has a great impact on the resulting residual stress [60–62]. This may explain the decrease into the compressive region in the hoop stress component measured by CM in the clad layer. Therefore, the compressive residual stresses measured at the weld clad surface and near-surface by XRD and ESPI provide complimentary data to those measured by DHD and CM.

## CLADDING-INDUCED RESIDUAL STRESS

During the course of this study, the greatest driver in material and process selection was to obtain a material combination that would generate compressive residual stress through weld cladding, particularly at the surface, the location at which operational stresses are highest.

In this paper, weld cladding of low-alloy 4330 carbon steel has been carried out using nickel-chromium–based superalloy IN625. Corrosion resistance offered by this alloy is advantageous; however, the tensile residual stress present in the clad layer will not aid in increasing resistance to fatigue failure [16,63].

The residual stress distribution obtained when weld cladding a low-alloy 4330 carbon steel substrate with 17-4 PH stainless steel has indicated the potential of obtaining compressive residual stress in the clad layer [21]. This indicates that material selection and the consequent interaction between clad and substrate materials is a key factor in the resulting residual stress distribution and, in turn, the effects on fatigue performance.

The mechanisms involved in the weld cladding process, including mechanical, thermal, and chemical mechanisms, give rise to residual stresses due to the joining of dissimilar materials, resulting in a complex residual stress distribution. The "shrink-fit" effect that occurs because of the shrinkage of the cladding relative to the substrate can give rise to

varying residual stress levels in the vicinity of the join because of variations in the heating and cooling cycles that occur during welding [7]. This results in varying levels of constraint on thermal expansion and contraction and, on a microscopic level, varying values of thermal properties in constituent phases that can generate varying residual strain fields [8]. This effect can be observed in the locations of maximum tensile and compressive residual stresses (see Tables 4 and 5, respectively), primarily in the XRD results. It can be seen that the maximum surface residual stresses measured are high in both tensile and compressive cases, particularly in the case of compressive residual stresses. This highlights significant variations in stress levels that can be observed using XRD, whether these are due to the residual stress generation mechanisms or measurement considerations. Joining of the materials can alter the material properties and microstructures through alloying and diffusion, giving rise to variations in residual stress that depend on measurement location in the clad layer or in the vicinity of the join [64]. It should be highlighted that the residual stress present in the original cylinder prior to cladding should not be neglected and that a stress-relief process should ideally be undertaken. Failing this, simulation of the residual stress due to forging, cutting, and machining should be carried out to quantify the stress-state prior to cladding. Maximum tensile hoop and axial residual stresses have been observed in the clad layer for all methods; however, discrepancies arise in the compressive stress component (Table 5). Variations due to the spatial and temporal variation in the cladding process could also arise, and therefore the location selected for measurement may not be fully representative of the entire component [26]. Such potential effects on the residual stress state in a component highlight the need for a highly controlled and optimized deposition process and the subsequent cooling to ensure residual stress generation is not only understood but also repeatable.

Although superalloy IN625 is a commonly utilized material in weld cladding, the tensile residual stress generated in the clad layer means that, from this perspective, there is potential for improvement to achieve an all-encompassing solution for a corrosion- and

### TABLE 4

Maximum tensile hoop and axial residual stresses and locations obtained using XRD, ESPI, DHD, and CM.

| Measurement Method | $\sigma_{hoop,\ max}$ | Location from Clad Surface (mm) | $\sigma_{axial,\ max}$ | Location from Clad Surface (mm) |
|---|---|---|---|---|
| XRD | 222 | 0 | 117 | 0 |
| ESPI | 253 | 1.05 | 407 | 1.2 |
| DHD | 312 | 0.6 | 333 | 0.6 |
| CM | 406 | 0.37 | 266 | 1 |

### TABLE 5

Maximum compressive hoop and axial residual stresses and locations obtained using XRD, ESPI, DHD, and CM.

| Measurement Method | $\sigma_{hoop,\ max}$ | Location from Clad Surface (mm) | $\sigma_{axial,\ max}$ | Location from Clad Surface (mm) |
|---|---|---|---|---|
| XRD | −546 | 0 | −605 | 0 |
| ESPI | −314 | 0.001 | −191 | 0.051 |
| DHD | −62 | 31 | −113 | 18 |
| CM | −130 | 1.9 | −57 | 19.5 |

erosion-resistant component with a favorable residual stress state. A tensile residual stress increases the mean stress, which will, in turn, increase the maximum stress level reached during service. In cyclic loading conditions, each cycle will cause an increase in fatigue damage through crack growth [65,66]. This will continue until the critical crack length results, leading then to crack propagation and component failure. For this reason, the presence of compressive residual stress is desired, such that crack growth will be limited because the crack face tends not to open during cyclic stress conditions.

## Conclusions

In this study, detailed analyses of residual stress distributions in a low-alloy 4330 carbon steel cylinder weld clad with nickel-chromium–based superalloy IN625 were obtained. The major observations of this work are as follows:

- The weld cladding of a low-alloy 4330 carbon steel cylinder with nickel-chromium–based superalloy IN625 is achieved using a hot-wire GTAW process. A clad layer is deposited on the outer diameter of the cylinder in two passes, resulting in a 6-mm-deep clad layer.
- The residual stresses throughout the component are measured using different techniques, including XRD, hole drilling based on ESPI, deep-hole drilling, and the contour method. These methods are shown to be highly complementary, gaining detailed residual stress distributions as a result of the weld cladding process.
- XRD and ESPI methods indicate compressive residual stresses that are present at the clad layer surface to a depth of around 0.35 mm, as indicated by ESPI. Hole drilling based on ESPI, deep-hole drilling, and the contour method indicate that tensile residual stresses are present further into the clad layer. Deep-hole drilling and the contour method allow distribution throughout the clad layer, at the interface, and throughout the substrate to be measured. It is shown that the balancing of the tensile residual stresses occurs with the presence of compressive residual stresses in the substrate. Both hoop and axial stress components are consistently the same in nature, with similar levels of stress throughout.
- This study highlights the need for a range of residual stress measurement techniques to gain knowledge of the residual stress distribution throughout the component.
- Weld cladding with superalloy IN625 has resulted in the presence of compressive residual stress on the surface and near-surface, counterbalanced by tensile residual stresses at greater depths.

## References

[1] Shi, L., Yan, Z., Liu, Y., Zhang, C., Qiao, Z., Ning, B., and Li, H., "Improved Toughness and Ductility in Ferrite/Acicular Ferrite Dual-Phase Steel through Intercritical Heat Treatment," *Mater. Sci. Eng., A*, Vol. 590, 2014, pp. 7–15, https://doi.org/10.1016/j.msea.2013.10.006

[2] Srivatsa, K., Srinivas, P., Balachandran, G., and Balasubramanian, V., "Improvement of Impact Toughness by Modified Hot Working and Heat Treatment in 13 %Cr Martensitic Stainless Steel," *Mater. Sci. Eng., A*, Vol. 677, 2016, pp. 240–251, https://doi.org/10.1016/j.msea.2016.09.045

[3] Genel, K., Demirkol, M., and Guelmez, T., "Corrosion Fatigue Behaviour of Ion Nitrided AISI 4140 Steel," *Mater. Sci. Eng., A*, Vol. 288, No. 1, 2000, pp. 91–100, https://doi.org/10.1016/S0921-5093(00)00835-2

[4] Hosford, W. F., *Mechanical Behavior of Materials*, Cambridge University Press, Cambridge, 2005, 425p.

[5] Webster, G. A. and Ezeilo, A. N., "Residual Stress Distributions and Their Influence on Fatigue Lifetimes," *Int. J. Fatigue*, Vol. 23, Suppl. 1, 2001, pp. 375–383, https://doi.org/10.1016/S0142-1123(01)00133-5

[6] Liu, A. F., *Mechanics and Mechanisms of Fracture: An Introduction*, ASM International, Materials Park, OH, 2005, 500p.

[7] Kandil, F. A., Lord, J. D., Fry, A. T., and Grant, P. V., *A Review of Residual Stress Measurement Methods– A Guide to Technique Selection*, NPL Report MATC(A)04, National Physical Laboratory, Teddington, UK, 2001, 42p.

[8] Withers, P. J. and Bhadeshia, H. K. D. H., "Residual Stress, Part 2– Nature and Origins," *Mater. Sci. Technol.*, Vol. 17, 2013, pp. 366–375, https://doi.org/10.1179/026708301101510087

[9] Leggatt, R. H., "Residual Stresses in Welded Structures," *Int. J. Press. Vessel. Pip.*, Vol. 85, No. 3, 2008, pp. 144–151, https://doi.org/10.1016/j.ijpvp.2007.10.004

[10] Stenberg, N. and Proudian, J., "Numerical Modelling of Turning to Find Residual Stresses," *Procedia CIRP*, Vol. 8, 2013, pp. 258–264, https://doi.org/10.1016/j.procir.2013.06.099

[11] Zhang, Z., Yang, Y., Li, L., Chen, B., and Tian, H., "Assessment of Residual Stress of 7050-T7452 Aluminum Alloy Forging Using the Contour Method," *Mater. Sci. Eng., A*, Vol. 644, 2015, pp. 61–68, https://doi.org/10.1016/j.msea.2015.07.018

[12] Dye, D., Conlon, K. T., and Reed, R. C., "Characterization and Modeling of Quenching-Induced Residual Stresses in the Nickel-Based Superalloy IN718," *Metall. Mater. Trans. A*, Vol. 35, No. 6, 2004, pp. 1703–1713, https://doi.org/10.1007/s11661-004-0079-7

[13] Coules, H. E., "Contemporary Approaches to Reducing Weld-Induced Residual Stress," *Mater. Sci. Technol.*, Vol. 29, No. 1, 2013, pp. 4–18, https://doi.org/10.1179/1743284712Y.0000000106

[14] García Navas, V., Gonzalo, O., Quintana, I., and Pirling, T., "Residual Stresses and Structural Changes Generated at Different Steps of the Manufacturing of Gears: Effect of Banded Structures," *Mater. Sci. Eng., A*, Vol. 528, No. 15, 2011, pp. 5146–5157, https://doi.org/10.1016/j.msea.2011.03.004

[15] Li, C. R., Zhang, Z. P., Zhang, Y. M., and Fang, Z. T., "Finite Element Simulative Analysis on the Influence of Solid-State Transformation on Welding Residual Stress," *Adv. Mater. Res.*, Vols. 785–786, 2013, pp. 1229–1235.

[16] Ramjaun, T. I., Stone, H. J., Karlsson, L., Gharghouri, M., Dalaei, K., Moat, R., and Bhadeshia, H. K. D. H., "Surface Residual Stresses in Multipass Welds Produced Using Low Transformation Temperature Filler Alloys," *Sci. Technol. Weld. Join.*, Vol. 19, No. 7, 2014, pp. 623–630, https://doi.org/10.1179/1362171814Y.0000000234

[17] Nitschke-Pagel, T. and Dilger, K., "Sources and Consequences of Residual Stresses due to Welding," *Mater. Sci. Forum*, Vols. 783–786, 2014, pp. 2777–2785.

[18] Silva, C. C., De Miranda, H. C., Motta, M. F., Farias, J. P., Afonso, C. R. M., and Ramirez, A. J., "New Insight on the Solidification Path of an Alloy 625 Weld Overlay," *J. Mater. Res. Technol.*, Vol. 2, No. 3, 2013, pp. 228–237, https://doi.org/10.1016/j.jmrt.2013.02.008

[19] Rae, W., Lomas, Z., Jackson, M., and Rahimi, S., "Measurements of Residual Stress and Microstructural Evolution in Electron Beam Welded Ti-6Al-4V Using Multiple Techniques," *Mater. Charact.*, Vol. 132, 2017, pp. 10–19, https://doi.org/10.1016/j.matchar.2017.07.042

[20] Easton, D., Wood, J., Rahimi, S., Galloway, A., Zhang, Y., and Hardie, C., "Residual Stress Generation in Brazed Tungsten Dissimilar Joints," *IEEE Trans. Plasma Sci.*, Vol. 44, No. 9, 2016, pp. 1625–1630, https://doi.org/10.1109/TPS.2016.2565205

[21] Benghalia, G., Rahimi, S., and Wood, J., "Measurements of Surface and Near-Surface Residual Stress in 4330 Low Alloy Carbon Steel Weld Clad Components," presented at the *Tenth International Conference on Residual Stresses 2016: ICRS-10*, Sydney, Australia, July 3–7, 2016, Materials Research Forum LLC, Millersville, PA, pp. 259–264.

[22] Rahimi, S., Wynne, B. P., and Baker, T. N., "Development of Microstructure and Crystallographic Texture in a Double-Sided Friction Stir Welded Microalloyed Steel," *Metall. Mater. Trans. A*, Vol. 48, No. 1, 2017, pp. 362–378, https://doi.org/10.1007/s11661-016-3833-8

[23] Gexia, Y. and Hongzhao, L., "An Analytical Solution of Residual Stresses for Shrink-Fit Two-Layer Cylinders after Autofrettage Based on Actual Material Behavior," *J. Pressure Vessel Technol.*, Vol. 134, No. 6, 2012, 061209, https://doi.org/10.1115/1.4006121

[24] Mahmoudi, A. H., Zheng, G., Smith, D. J., Truman, C. E., and Pavier, M. J., "A Procedure to Measure Biaxial Near Yield Residual Stresses Using the Deep Hole Drilling Technique," *Exp. Mech.*, Vol. 53, No. 7, 2013, pp. 1223–1231, https://doi.org/10.1007/s11340-013-9729-2

[25] Hutchings, M. T. and Krawitz, A. D., *"Measurement of Residual and Applied Stress Using Neutron Diffraction,"* Nato Science Series E, Vol. 216, Springer, the Netherlands, 1992, 588p.

[26] Taljat, B., Zacharia, T., Wang, X.-L., Keiser, J. R., Swindeman, R. W., Feng, Z., and Jirinec, M. J., "Numerical Analysis of Residual Stress Distribution in Tubes with Spiral Weld Cladding," *Weld. J.*, Vol. 77, No. 8, 1998, pp. 328–335.

[27] Smith, M. C., Muransky, O., Goodfellow, A., Kingston, E., Freyer, P., Marlette, S., Wilkowski, G. M., Brust, B., and Shim, D.-J., "The Impact of Key Simulation Variables on Predicted Residual Stresses in Pressuriser Nozzle Dissimilar Metal Weld Mock-Ups: Part 2—Comparison of Simulation and Measurements," presented at the *ASME 2010 Pressure Vessels and Piping Division/K-PVP Conference*, Bellevue, WA, July 18–22, 2010, ASME, New York, pp. 1495–1511.

[28] Dennis, R. J., Leggatt, N. A., Smith, M. C., and Bouchard, P. J., "R6 Weld Modelling Guidelines: Application to Groove Weld Worked Example," presented at the *ASME 2010 Pressure Vessels and Piping Division/K-PVP Conference*, Bellevue, WA, July 18–22, 2010, ASME, New York, pp. 1435–1448.

[29] Zhu, X. K. and Chao, Y. J., "Effects of Temperature-Dependent Material Properties on Welding Simulation," *Comput. Struct.*, Vol. 80, No. 11, 2002, pp. 967–976, https://doi.org/10.1016/S0045-7949(02)00040-8

[30] Liu, S., Liu, W., Harooni, M., Ma, J., and Kovacevic, R., "Real-Time Monitoring of Laser Hot-Wire Cladding of Inconel 625," *Opt. Laser Technol.*, Vol. 62, 2014, pp. 124–134, https://doi.org/10.1016/j.optlastec.2014.03.007

[31] Maltin, C. A., Galloway, A. M., and Mweemba, M., "Microstructural Evolution of Inconel 625 and Inconel 686CPT Weld Metal for Clad Carbon Steel Linepipe Joints: A Comparator Study," *Metall. Mater. Trans. A*, Vol. 45, No. 8, 2014, pp. 3519–3532, https://doi.org/10.1007/s11661-014-2308-z

[32] Zahrani, E. M. and Alfantazi, A. M., "Hot Corrosion of Inconel 625 Overlay Weld Cladding in Smelting Off-Gas Environment," *Metall. Mater. Trans. A*, Vol. 44, No. 10, 2013, pp. 4671–4699, https://doi.org/10.1007/s11661-013-1803-y

[33] Zahrani, E. M. and Alfantazi, A. M., "High Temperature Corrosion and Electrochemical Behavior of INCONEL 625 Weld Overlay in PbSO4-Pb3O4–PbCl2-CdO–ZnO Molten Salt Medium," *Corros. Sci.*, Vol. 85, 2014, pp. 60–76, https://doi.org/10.1016/j.corsci.2014.03.034

[34] Rozmus-Górnikowska, M., Cieniek, Ł., Blicharski, M., and Kusiński, J., "Microstructure and Microsegregation of an Inconel 625 Weld Overlay Produced on Steel Pipes by the Cold Metal Transfer Technique," *Arch. Metall. Mater.*, Vol. 59, No. 3, 2014, pp. 1081–1084, https://doi.org/10.2478/amm-2014-0185

[35] Silva, C. C., Afonso, C. R. M., Ramirez, A. J., Motta, M. F., de Miranda, H. C., and Farias, J. P., "Evaluation of the Corrosion Resistant Weld Cladding Deposited by the TIG Cold Wire Feed Process," *Mater. Sci. Forum*, Vols. 783–786, 2014, pp. 2822–2827.

[36] Abioye, T. E., McCartney, D. G., and Clare, A. T., "Laser Cladding of Inconel 625 Wire for Corrosion Protection," *J. Mater. Process. Technol.*, Vol. 217, 2015, pp. 232–240, https://doi.org/10.1016/j.jmatprotec.2014.10.024

[37] Xing, X., Di, X., and Wang, B., "The Effect of Post-Weld Heat Treatment Temperature on the Microstructure of Inconel 625 Deposited Metal," *J. Alloys Compd.*, Vol. 593, 2014, pp. 110–116, https://doi.org/10.1016/j.jallcom.2013.12.224

[38] Fitzpatrick, M. E., Fry, A. T., Holdway, P., Kandil, F. A., Shackleton, J., and Suominen, L., *Determination of Residual Stresses by X-Ray Diffraction– Issue 2, Measurement Good Practice Guide No. 52*, National Physical Laboratory, Teddington, UK, 2005, 68p.

[39] Jones, R. and Leendertz, J. A., "Elastic Constant and Strain Measurements Using a Three Beam Speckle Pattern Interferometer," *J. Phys. E: Sci. Instrum.*, Vol. 7, No. 8, 1974, pp. 653–657, https://doi.org/10.1088/0022-3735/7/8/020

[40] Leggatt, R. H., Smith, D. J., Smith, S. D., and Faure, F., "Development and Experimental Validation of the Deep Hole Method for Residual Stress Measurement," *J. Strain Anal. Eng. Des.*, Vol. 31, No. 3, 2007, pp. 177–186, https://doi.org/10.1243/03093247V313177

[41] George, D., Kingston, E., and Smith, D. J., "Measurement of Through-Thickness Stresses Using Small Holes," *J. Strain Anal. Eng. Des.*, Vol. 37, No. 2, 2005, pp. 125–139, https://doi.org/10.1243/0309324021514899

[42] Mahmoudi, A. H., Hossain, S., Truman, C. E., Smith, D. J., and Pavier, M. J., "A New Procedure to Measure Near Yield Residual Stresses Using the Deep Hole Drilling Technique," *Exp. Mech.*, Vol. 49, No. 4, 2009, pp. 595–604, https://doi.org/10.1007/s11340-008-9164-y

[43] Goudar, D. M., Truman, C. E., and Smith, D. J., "Evaluating Uncertainty in Residual Stress Measured Using the Deep-Hole Drilling Technique," *Strain*, Vol. 47, No. 1, 2011, pp. 62–74, https://doi.org/10.1111/j.1475-1305.2009.00620.x

[44] Prime, M. B., "Cross-Sectional Mapping of Residual Stresses by Measuring the Surface Contour after a Cut," *J. Eng. Mater. Technol.*, Vol. 123, No. 2, 2001, pp. 162–168, https://doi.org/10.1115/1.1345526

[45] Prime, M. B., "Contour Method Advanced Applications: Hoop Stresses in Cylinders and Discontinuities," *Eng. Appl. Residual Stress*, Vol. 8, 2011, pp. 13–28.

[46] Hosseinzadeh, F., Ledgard, P., and Bouchard, P. J., "Controlling the Cut in Contour Residual Stress Measurements of Electron Beam Welded Ti-6Al-4V Alloy Plates," *Exp. Mech.*, Vol. 53, No. 5, 2013, pp. 829–839, https://doi.org/10.1007/s11340-012-9686-1

[47] Hosseinzadeh, F. and Bouchard, P. J., "Mapping Multiple Components of the Residual Stress Tensor in a Large P91 Steel Pipe Girth Weld Using a Single Contour Cut," *Exp. Mech.*, Vol. 53, No. 2, 2013, pp. 171–181, https://doi.org/10.1007/s11340-012-9627-z

[48] DeWald, A. T. and Hill, M. R., "Multi-Axial Contour Method for Mapping Residual Stresses in Continuously Processed Bodies," *Exp. Mech.*, Vol. 46, 2006, pp. 473–490, https://doi.org/10.1007/s11340-006-8446-5

[49] Pagliaro, P., Prime, M. B., Robinson, J. S., Clausen, B., Swenson, H., Steinzig, M., and Zuccarello, B., "Measuring Inaccessible Residual Stresses Using Multiple Methods and Superposition," *Exp. Mech.*, Vol. 51, No. 7, 2011, pp. 1123–1134, https://doi.org/10.1007/s11340-010-9424-5

[50] Pollard, J. D., Rahimi, S., Watford, A., Jackson, M., and Wynne, B. P., "The Determination of Residual Stress in Extruded Ti-6Al-4V by Contour Method and Finite Element Analysis," presented at the *13th World Conference on Titanium*, San Diego, CA, Aug. 16–20, 2015, The Minerals, Metals and Materials Society, Pittsburgh, PA, pp. 305–310.

[51] Prime, M. B. and DeWald, A. T., "The Contour Method," *Practical Residual Stress Measurement Methods*, G. S. Schajer, Ed., John Wiley and Sons Ltd, Hoboken, NJ, 2013, pp. 109–138.

[52] Schnier, G., Wood, J., and Galloway, A., "An Experimental Validation of Residual Stresses in Weld Clad Pipelines," presented at the *Fifth International Conference on Structural Engineering*, Mechanics and Computation, Cape Town, South Africa, Sept. 2–4, 2013, UNISDR, Geneva, Switzerland, pp. 613–617.

[53] Schnier, G., Wood, J., and Galloway, A., "Investigating the Effects of Process Variables on the Residual Stresses of Weld and Laser Cladding," *Adv. Mater. Res.*, Vol. 996, 2014, pp. 481–487, https://doi.org/10.4028/www.scientific.net/AMR.996.481

[54] Prime, M. B. and Steinzig, M. L., "Beyond the Streetlight Effect: A United Future for Relaxation and Diffraction Methods for Residual Stress Measurement," *Adv. Mater. Res.*, Vol. 996, 2014, pp. 234–242, https://doi.org/10.4028/www.scientific.net/AMR.996.234

[55] Genel, K., Demirkol, M., and Çapa, M., "Effect of Ion Nitriding on Fatigue Behaviour of AISI 4140 Steel," *Mater. Sci. Eng. A*, Vol. 279, Nos. 1–2, 2000, pp. 207–216, https://doi.org/10.1016/S0921-5093(99)00689-9

[56] Tomota, Y., Daikuhara, S., Nagayama, S., Sugawara, M., Ozawa, N., Adachi, Y., Harjo, S., and Hattori, S., "Stress Corrosion Cracking Behavior at Inconel and Low Alloy Steel Weld Interfaces," *Metall. Mater. Trans. A*, Vol. 45, No. 13, 2014, pp. 6103–6117, https://doi.org/10.1007/s11661-014-2560-2

[57] Rahimi, S., Mehrez, K., and Marrow, T. J., "Effect of Surface Machining on Intergranular Stress Corrosion Cracking (IGSCC) in Sensitised Type 304 Austenitic Stainless Steel," *Corros. Eng. Sci. Technol.*, Vol. 51, No. 5, 2016, pp. 383–391, https://doi.org/10.1080/1478422X.2015.1122295

[58] Rahimi, S. and Marrow, T. J., "Effects of Orientation, Stress and Exposure Time on Short Intergranular Stress Corrosion Crack Behaviour in Sensitised Type 304 Austenitic Stainless Steel," *Fatigue Fract. Eng. Mater. Struct.*, Vol. 35, No. 4, 2012, pp. 359–373, https://doi.org/10.1111/j.1460-2695.2011.01627.x

[59] Olson, M. D., DeWald, A. T., Prime, M. B., and Hill, M. R., "Estimation of Uncertainty for Contour Method Residual Stress Measurements," *Exp. Mech.*, Vol. 55, No. 3, 2015, pp. 577–585, https://doi.org/10.1007/s11340-014-9971-2

[60] Singh, L., Shah, V., and Singh, N. K., "Study The Influence of TIG Welding Parameters On Weld Characteristics Of 5083 Aluminum Alloy," *Int. J. Eng. Sci. Innov. Technol.*, Vol. 2, No. 5, 2013, pp. 462–468.

[61] Leal, J. E. S., Costa, T. F., and Arencibia, R. V., "Evaluation of Geometric Quality of Weld Beads in the Joining of Carbon Steel Pipelines with Single Pass," *J. Power Energy Eng.*, Vol. 1, No. 7, 2013, pp. 1–5, https://doi.org/10.4236/jpee.2013.17001

[62] Smith, M. C. and Smith, A. C., "NeT Bead-on-Plate Round Robin: Comparison of Residual Stress Predictions and Measurements," *Int. J. Press. Vessel. Pip.*, Vol. 86, No. 1, 2009, pp. 79–95, https://doi.org/10.1016/j.ijpvp.2008.11.017

[63] Benachour, M., Benguediab, M., and Benachour, N., "Notch Fatigue Crack Initiation and Propagation Life under Constant Amplitude Loading through Residual Stress Field," *Adv. Mater. Res.*, Vol. 682, 2013, pp. 17–24, https://doi.org/10.4028/www.scientific.net/AMR.682.17

[64] Šohaj, P. and Jan, V., "Local Changes of Microhardness in Dissimilar Weld Joints after High Temperature Exposure," *Key Eng. Mater.*, Vol. 586, 2013, pp. 249–252, https://doi.org/10.4028/www.scientific.net/KEM.586.249

[65] Pan, L., Athreya, B. P., Forck, J. A., Huang, W., Zhang, L., Hong, T., Li, W., Ulrich, W., and Mach, J. C., "Welding Residual Stress Impact on Fatigue Life of a Welded Structure," *Weld. World*, Vol. 57, No. 5, 2013, pp. 685–691, https://doi.org/10.1007/s40194-013-0067-x

[66] Zerbst, U., Ainsworth, R. A., Beier, H. T., Pisarski, H., Zhang, Z. L., Nikbin, K., Nitschke-Pagel, T., Münstermann, S., Kucharczyk, P., and Klingbeil, D., "Review on Fracture and Crack Propagation in Weldments– A Fracture Mechanics Perspective," *Eng. Fract. Mech.*, Vol. 132, 2014, pp. 200–276, https://doi.org/10.1016/j.engfracmech.2014.05.012